Graphene thermocouple fabricated on a flexible and transparent substrate

Downloaded from: https://research.chalmers.se, 2025-12-04 22:59 UTC

Citation for the original published paper (version of record):
Nam, Y., Gu, D., Khan, M. et al (2024). Graphene thermocouple fabricated on a flexible and transparent substrate. AIP Advances, 14(6). http://dx.doi.org/10.1063/5.0203178

N.B. When citing this work, cite the original published paper.

research.chalmers.se offers the possibility of retrieving research publications produced at Chalmers University of Technology. It covers all kind of research output: articles, dissertations, conference papers, reports etc. since 2004. research.chalmers.se is administrated and maintained by Chalmers Library

(article starts on next page)

AIP Advances

RESEARCH ARTICLE | JUNE 05 2024

Graphene thermocouple fabricated on a flexible and transparent substrate

Youngwoo Nam ; Daewon Gu ; Munis Khan ; August Yurgens

Check for updates

AIP Advances 14, 065012 (2024)
https://doi.org/10.1063/5.0203178

View Online
Export Citation

24 June 2024 10:38:33

AIP Advances
Special Topic: Machine Vision, Optical Sensing and Measurement
Submit Today
AIP Publishing

AIP Publishing

Graphene thermocouple fabricated on a flexible and transparent substrate

Cite as: AIP Advances 14, 065012 (2024); doi: 10.1063/5.0203178
Submitted: 17 March 2024 • Accepted: 17 May 2024 •
Published Online: 5 June 2024

View Online Export Citation CrossMark

Youngwoo Nam,[1,a)] Daewon Gu,[1] Munis Khan,[2] and August Yurgens[2]

AFFILIATIONS

[1] Department of Physics, Gyeongsang National University, Jinju 52828, South Korea
[2] Department of Microtechnology and Nanoscience, Chalmers University of Technology, SE-412 96 Göteborg, Sweden

[a)] **Author to whom correspondence should be addressed:** youngwoo.nam@gnu.ac.kr

ABSTRACT

We demonstrate the realization of reliable, high-quality, micro-sized graphene-based field-effect devices on a flexible and transparent substrate, ethylene vinyl acetate (EVA)/polyethylene terephthalate (PET), using a convenient hot-press lamination transfer and employing parylene-N as a dielectric material for gating. Using this technique, we fabricate a graphene thermocouple on the EVA/PET substrate. Specifically, the graphene is patterned in a U-shape, and its legs are equipped with two independent top gates. Full control of the carrier density and type by electrostatic gating in the two graphene regions allow the formation of a thermocouple layout, exhibiting an enlarged thermovoltage signal when the two regions are doped with opposite types of carriers and leading to a maximum sensitivity with a thermopower of ~73 μV/K. This agrees well with the working principle of thermocouple, and it proves the good compatibility and functionality of the graphene thermocouple on the EVA/PET substrate. Our findings suggest possible applications for producing scalable and reliable graphene-based electronic devices on flexible and transparent substrates in a simple way.

© 2024 Author(s). All article content, except where otherwise noted, is licensed under a Creative Commons Attribution (CC BY) license (https://creativecommons.org/licenses/by/4.0/). https://doi.org/10.1063/5.0203178

24 June 2024 10:38:33

INTRODUCTION

High-quality graphene-based electronic devices are typically prepared on silicon substrates because the rigidity of the substrate easily allows for structural integrity and stable working conditions for the devices. This robust substrate is particularly suitable for studying the fundamental physics associated with the intrinsic electronic properties of graphene or finding new physics systems stemming from engineered electronic properties with van der Waals-bonded heterostructures by stacking graphene layers in a controlled manner or combining them with other two-dimensional materials.[1–4] Graphene flakes are usually obtained by mechanical exfoliation to fabricate such a high-quality device, although their size is limited to several tens of microns at most. In this case, the graphene layer exfoliated onto the proper thickness of the oxidized silicon surface is highly visible with an optical microscope, enabling the identification of the layer thickness up to the heptalayer owing to the clear contrast difference.[5] In addition, the conducting silicon substrate underneath can be easily employed as a back-gate electrode in a field-effect configuration, which controls the carrier density and type by applying a gate voltage between the graphene and the substrate.[6,7]

Considering the commercial applications of graphene-based field-effect devices, a polyethylene terephthalate (PET) substrate is a good candidate and is suitable for various environments because it is flexible and transparent. Transferring large-area CVD-grown graphene onto the PET substrate can make device production straightforward and scalable, facilitating mass production.[8,9] Compared with the highest-quality graphene devices prepared on a rigid substrate (for example, devices on a silicon substrate by encapsulating graphene with hexagonal boron nitride),[10,11] the mobility of graphene devices fabricated in this way is known to be 1–2 orders of magnitude lower. However, they are still sufficiently good for use as conductive films for display and sensor applications. One drawback is the necessity of finding a well-suited dielectric material with the PET substrate for electrostatic gating the graphene channel.

This study demonstrates the realization of reliable, high-quality graphene field-effect devices on a typical lamination film, PET, covered with a glue layer of ethylene vinyl acetate (EVA), using an office hot-press laminator.[12–18] Importantly, we found that parylene-N is

© Author(s) 2024

an appropriate dielectric material for graphene devices on EVA/PET substrates to facilitate field effects. Based on this technique, we fabricated a graphene thermocouple junction on the EVA/PET substrate by implementing two separate gates on each leg of the U-shaped etched graphene to tune the carrier density and type independently, thus forming a typical thermocouple layout.

METHODS

Using a commercial hot-press laminator, large-area graphene synthesized on a copper foil by the CVD method was laminated onto the EVA/PET film (150 μm thick). After lamination, the copper foil attached to the film was etched in 30% nitric acid. Subsequently, the metal electrodes for the source, drain, and voltage probes [denoted as S, D, and 1–4, respectively, in Fig. 1(b)] were defined on the film using photolithography and metal deposition (Au/Ti = 100 nm/10 nm) followed by the shaping of the graphene channel by oxygen plasma etching. Then, ~180 nm-thick parylene-N acting as a dielectric layer was conformally deposited by the CVD method. Finally, the top gate electrodes [marked as G in Fig. 1(b)] were fabricated using the same microfabrication process as the bottom electrodes (source, drain, and voltage probes), and parylene-N covered on the contact pads of bottom electrodes was selectively etched by oxygen plasma to make electrical connections. The cross-sectional schematic of the final device is shown in Fig. 1(a). Devices are annealed at 65 °C under a nitrogen flow for several hours after etching the graphene and immediately before loading devices into the vacuum chamber to remove possible chemical impurities from the copper etchant and lithography process.[18] Detailed characterization of the graphene layer itself on the EVA/PET film can be found in our previous work.[18]

The electrical resistance was measured using a conventional low-frequency lock-in technique, whereas the thermovoltage was measured using the steady-state DC method or low-frequency AC method.[19] Both measurements were performed at room temperature in a vacuum environment to avoid unwanted doping effects from moisture in the air and to prevent uncontrolled heat dissipation.

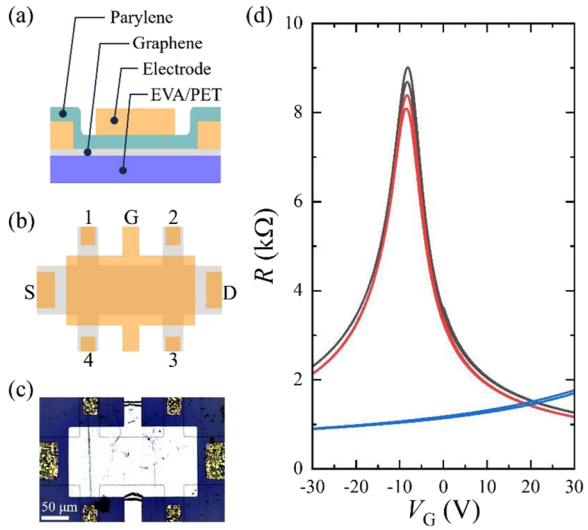

FIG. 1. (a) Cross-sectional schematic of a device (not to scale). Using a conventional hot-press laminator, the CVD-grown graphene is transferred to an EVA/PET substrate, and metal electrodes [denoted as S, D, and 1–4 in (b)] are defined. After shaping graphene by oxygen plasma etching, parylene-N covers it and serves as a dielectric layer. Subsequently, a gate electrode (denoted as G) is deposited. (b) In-plane device design: standard Hall-bar geometry equipped with a top gate on the graphene channel. (c) Corresponding optical microscope image of the completed graphene Hall-bar device on an EVA/PET substrate. The relatively rough surface of the substrate and weak adhesion of metal to parylene-N cause wrinkles in the electrodes. (d) Gate voltage (V_G) dependence of four-terminal resistances (R) measured by applying current between the source (S) and drain (D) electrodes and probing voltage between contacts 1 and 2 (contacts 3 and 4) is shown in the black (red) curve. In both cases, clear peaks are seen at nearly the same gate voltage (corresponding to the charge neutrality point), indicating that the graphene quality on EVA/PET is homogeneous and their interface is uniformly clean. Based on the curves, field-effect mobility is estimated to be ≈4000 cm^2 V^{-1} s^{-1}. The blue curve is obtained from another graphene field-effect device prepared by the same fabrication process in the same geometry but using the CVD-grown graphene placed on a PET substrate by a PMMA-assisted wet transfer technique. In this case, it is highly p-doped, most likely due to process contamination residues introduced during the wet transfer process.

RESULTS AND DISCUSSION

Graphene was shaped in a standard Hall-bar geometry, which allows us to confirm longitudinal and transverse resistances in multiple contact configurations to find out the quality of the graphene devices fabricated on the EVA/PET substrate. Specifically, this leads us to estimate the mobility and verify the homogeneity of the graphene transferred onto the substrate. Figure 1(b) displays the top view of the actual device design, and Fig. 1(c) shows an optical microscope image of the completed device. Fine wrinkles are observed in the bottom electrodes [corresponding to S, D, and 1-4 in Fig. 1(b)], which originated from the rough surface of the substrate caused by the EVA glue. Wrinkles were also apparent in the top-gate lead lines, probably because of the partially poor adhesion of metals and parylene-N. Such untidiness can be improved by optimizing the fabrication conditions.

Figure 1(d) shows the gate voltage (V_G) dependence of the four-terminal resistance measured by applying a current between the source (S) and drain (D) electrodes and probing voltage between contacts 1 and 2 and contacts 3 and 4, corresponding to the black and red curves, respectively. The two curves are almost identical, and clear peaks are observed with little hysteresis when the gate voltage is near the charge neutrality point (CNP) $V_{CNP} \approx -8$ V, indicating that the quality of graphene transferred onto the EVA/PET substrate is homogeneous and that large potential fluctuations induced by charged impurities are absent. The CNP position reveals it to be slightly N-type doped by carrier density $n \approx 6 \times 10^{11}$ cm^{-2}, most likely due to electron transfer from parylene-N to graphene.[17,18,20] Based on the sharpness of the curves, field-effect mobility is estimated to be ≈4000 cm^2 V^{-1} s^{-1}, while gate coupling constant α [$= n/(V_G - V_{CNP}) \approx 7.5 \times 10^{10}$ cm^{-2} V^{-1}] is obtained via Hall effect measurement. Using the same fabrication technique, for comparison, we prepared a same-sized Hall-bar device on commercial CVD-grown graphene placed directly on a PET film using the PMMA-assisted wet transfer technique. This device was found to be excessively p-type doped such that the CNP was not observed within our gate voltage range [blue curve in Fig. 1(d)], most likely

24 June 2024 10:38:33

© Author(s) 2024

due to unwanted contamination by the chemical residue introduced during the wet transfer process.[21,22] This implies that our fabrication method using an EVA/PET substrate with hot-press lamination transfer and employing parylene-N as a dielectric layer provides sufficiently high-quality and uniform devices with reduced process impurities.

Using such an impurity-free production technique, a graphene-based thermoelectric device is fabricated on the EVA/PET substrate. The thermoelectric effect refers to voltage development resulting from temperature difference.[23] This occurs because the temperature gradient creates an imbalance in charge distribution through the diffusion of carriers from hotter to colder positions, resulting in voltage generation between the two positions. This temperature gradient-induced voltage (i.e., thermal electromotive force) is often called thermovoltage and is linearly proportional to the temperature difference in the linear response transport regime,

$$\Delta V = -S\Delta T,$$

where $\Delta T \equiv T^i - T^j$ is an imposed temperature difference between positions i and j at the material and $\Delta V \equiv V^i - V^j$ is a corresponding developed voltage measured between the same positions i and j. Here, for the sake of convenience, i and j are assigned to hot (H) and cold (C) positions to give a positive value in ΔT, that is, $\Delta T \equiv T^H - T^C > 0$. As to $\Delta V \equiv V^H - V^C$, its sign depends on the type of carriers in the material such that $\Delta V > 0$ for electrons and $\Delta V < 0$ for holes. S defines the linear proportionality between ΔV and ΔT, and it is often called the thermopower or Seebeck coefficient. Based on the sign relationship between ΔT and ΔV, the sign of S directly represents the type of majority carriers in the material: $S < 0$ for electrons and $S > 0$ for holes. Microscopically, S is a fundamental physical characteristic that manifests the intrinsic properties of a material associated with the change of electronic density of states near the Fermi energy level.[23]

Thermocouples are widely used temperature sensors that employ the thermoelectric effects and consist of two dissimilar metal wires, A and B, that possess thermopowers S_A and S_B, as shown in Fig. 2(a). Their ends are linked and form a junction, which

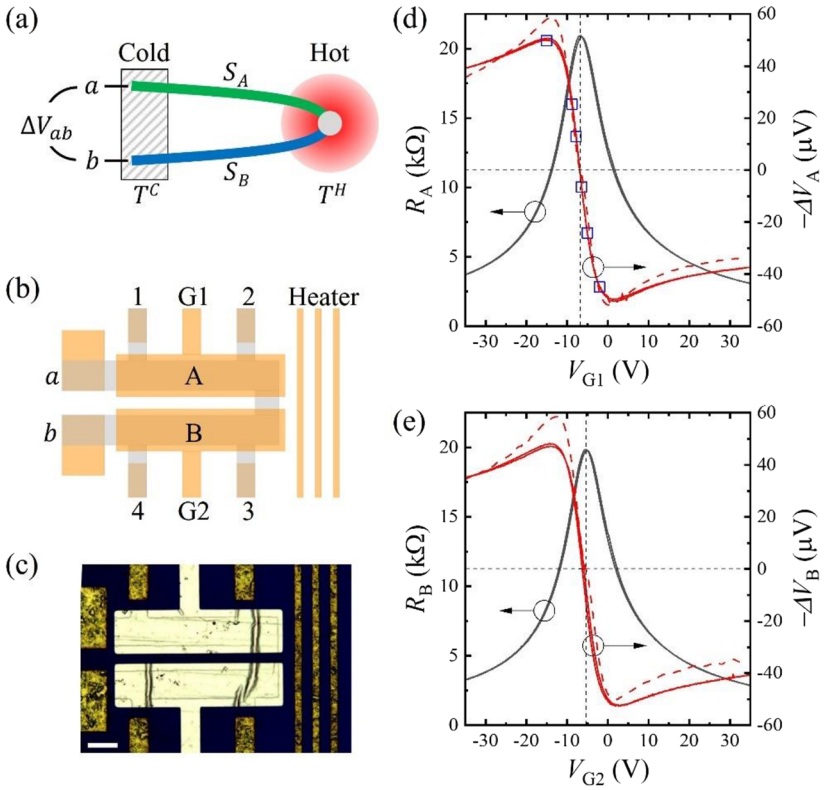

FIG. 2. (a) Schematic concept of a thermocouple comprising two dissimilar wires with different thermopowers, S_A and S_B. The junction of each wire plays a role in sensing temperature, while their open ends, a and b, are fixed at a thermal reservoir (shaded area) maintained at a constant temperature and connected to a voltmeter. The temperature difference along the wires induces a thermovoltage ΔV_{ab} between their open ends. (b) Device design of a graphene thermocouple. Single material graphene is patterned in a U-shape (gray area) and separated into two regions, A and B, to mimic the configuration of a thermocouple in (a). Carrier density and polarity in the two regions are independently controlled by two top gates, G1 and G2. (c) Corresponding optical microscope image of the completed device on an EVA/PET substrate. The scale bar is 50 μm. (d) and (e) Gate voltage dependence of resistance (R) and thermovoltage (ΔV) measured separately in each graphene region A and B. In both cases, clear resistance peaks and thermovoltage sign reversal are evident at similar charge neutrality points. Red dashed lines are fits of the thermovoltage using the Mott formula with a temperature difference $\Delta T = 1.5$ K.

24 June 2024 10:38:33

© Author(s) 2024

senses temperature. The remaining free ends, a and b, are attached to a thermal reservoir maintained at a constant temperature and connected to a voltmeter to measure the thermovoltage under open-circuit conditions. When heating the junction by $\Delta T(\equiv T^H - T^C > 0)$, that is, assuming that the temperature at the junction (reservoir) is T^H (T^C), the thermovoltage between their ends reads

$$\begin{aligned}\Delta V_{ab}(\equiv V_a - V_b) &= (V_A^C - V_A^H) + (V_B^H - V_B^C)\\ &= -S_A(T^C - T^H) - S_B(T^H - T^C)\\ &= (S_A - S_B)\Delta T.\end{aligned}$$

Here, we see that ΔV_{ab} includes two competing thermovoltage contributions from each metal wire. This explains why thermocouples are typically comprised of two materials with different thermopowers and opposite signs.

Using this concept, we fabricated a gate-controlled graphene thermocouple on a flexible and transparent substrate. To this end, graphene was patterned in a U-shape on EVA/PET substrates, and its two legs were equipped with top gates [denoted as G1 and G2 in Fig. 2(b)]. We exploited the property that the sign and magnitude of the thermopower of graphene can be easily tuned by varying the gate voltage; for example, the sign of the thermopower can be $S > 0$ ($S < 0$) by setting the gate voltage to be $V_G < V_{CNP}$ ($V_G > V_{CNP}$) because the majority carrier type is changed to hole (electron).[24–26] Full control of the two independent gates converted a single material graphene strip into two regions, A and B, analogous to the thermocouple layout. Figure 2(c) shows an optical microscope image of the graphene thermocouple device. The thin metal line on the right side is a resistive heater that generates a temperature gradient along the graphene thermocouple via joule heating. We note that our thermocouple format is different from previously reported ones that rely on a rigid substrate[27] or uncontrolled thermopower of graphene.[28–30]

The gate voltage dependences of the resistance and thermovoltage for graphene regions A and B are shown in Figs. 2(d) and 2(e), respectively. In both cases, a clear resistance peak and sign reversals of the thermovoltage were apparent at the CNP as the carrier polarity changed. In the plots, thermovoltage signs are reversed as $-\Delta V(= V^C - V^H)$ to have the same sign with the thermopower of graphene; that is, $-\Delta V_A = V_1 - V_2$ and $-\Delta V_B = V_4 - V_3$ are defined to indicate the thermovoltage of regions A and B, respectively. In principle, the measured voltages include the thermovoltage developed along metallic voltage leads. This means that thermovoltage contributions from voltage leads ($S_{Au}\Delta T$) must be added to the measured ones to extract thermovoltage solely from graphene. However, we disregarded this because the thermopower of gold (S_{Au}) is usually 1–2 orders of magnitude smaller than that of graphene at room temperature. The thermovoltage can be analyzed quantitatively using the semiclassical Mott relation, $S_{Mott} = (\pi^2 k_B^2 T/3|e|)(1/R)(dR/dV_G)(dV_G/dE_F)$, where e is the electron charge and k_B is the Boltzmann constant.[24,25] In detail, S_{Mott} is calculated using the measured gate voltage-dependent resistance and the linear dispersion relation of graphene, yielding $dV_G/dE_F = (2/\hbar v_F)\sqrt{(|\Delta V_G|/\alpha\pi)}$, where $\hbar$ is Planck's constant, the Fermi velocity $v_F = 10^6$ m/s, and $\Delta V_G = V_G - V_{CNP}$. Using a temperature difference ΔT as a fitting parameter, the measured thermovoltage is fitted with $S_{Mott}\Delta T$ [red dashed lines in Figs. 2(d) and 2(e)], allowing us to estimate that $\Delta T \approx 1.5$ K.

To validate that the measured voltage arises solely from the thermal effects initiated by heating the EVA/PET substrate using a microheater, we monitored the change in voltage as a function of the heater current while fixing the gate voltage at multiple values, which are marked by the empty squares in Fig. 2(d). For all gate voltages, they exhibited a clear quadratic dependence on the applied heater current (Fig. 3). This agrees with the thermal conduction mechanism, in which the magnitude of the induced temperature difference is linearly proportional to the heating power, coupled with the thermal conductance of the EVA/PET substrate. Therefore, we can infer that the voltage signals measured in the experiment are associated with thermoelectric effects.

To analyze the performance of the graphene thermocouple systematically, we measured both resistance and thermovoltage of the entire device, including regions A and B, by simultaneously varying the two gate voltages. Fully independent control of the two gates allowed us to investigate these quantities for various combinations of carrier density and polarity in each region. In the resistance measurement [Fig. 4(a)], a bias current was applied between contacts a and b, and the voltage was measured between contacts 1 and 4. Therefore, the total resistance (R_{tot}) is expected to be a simple sum of the resistance from the two regions with a finite constant term, which is mostly contributed by the ungated region in between. Figure 4(a) shows the total resistance as a function of the two gate voltages, exhibiting four areas divided by two intersecting ridges of high resistance (gray dashed lines). Those two high resistance lines occur when the gate voltages are tuned at the CNP in either region A or B because the resistance from each region is maximum at the CNP and decreases monotonically as the gate voltage moves away from the CNP, leading to four characteristic areas: p–n, n–n, n–p, and p–p, marked based on the combination of carrier polarity in regions A and B.

The thermovoltage between contacts 1 and 4 was measured as a function of the two gate voltages [as shown in Fig. 4(b)].

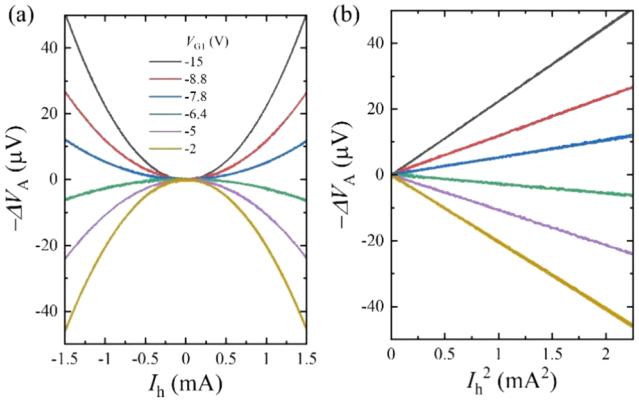

FIG. 3. Thermovoltage measured as a function of (a) heater current (I_h) and (b) square of heater current (I_h^2) at fixed gate voltage values denoted as empty squares in Fig. 2(d). The quadratic relationship between thermovoltage and heater current directly validates that our results rely on thermoelectric origin associated with heat conduction; that is, the magnitude of the induced temperature difference is linearly proportional to the heating power coupled by the thermal conductance of the EVA/PET substrate.

24 June 2024 10:38:33

© Author(s) 2024

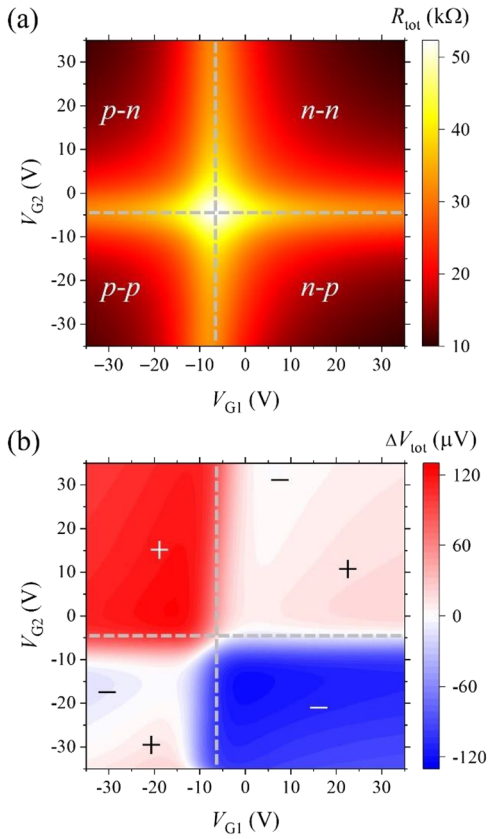

FIG. 4. 2D color maps of resistance (R_{tot}) and thermovoltage (ΔV_{tot}) measured in a graphene thermocouple as a function of two gate voltages, V_{G1} and V_{G2}, that control the carrier density and polarity of two graphene regions independently. (a) Resistance shows two high resistance ridges (gray dashed lines) associated with the charge neutrality points of each graphene region. Depending on the combination of carrier polarity in regions A and B, four distinct areas are apparent, marked as p–n, n–n, n–p, and p–p. (b) Thermovoltage displays an enlarged magnitude in the p–n and n–p combinations [the same border lines in (a) are drawn] because it is determined by subtraction of the two thermovoltages arising from each graphene region as in the thermocouple. The two other areas corresponding to p–p and n–n show a relatively small thermovoltage, as expected. An alternating sign reversal (marked as + and − for the sign) is observed due to the non-monotonic gate voltage dependence of the thermopower away from the charge neutrality point in graphene.

The total thermovoltage (ΔV_{tot}) is the subtraction of contributions from each region, as in the case of the thermocouple, and the ungated graphene region in the middle minimally affects the resulting thermovoltage because the symmetric temperature profile on it creates negligible thermoelectric effects. The thermovoltage shows an enlarged magnitude in p–n and n–p configurations with a maximum of 126 μV because ΔV_A and ΔV_B are comparable magnitudes with opposite signs, which corresponds to a maximum sensitivity with thermopower, $S_{max} = \max(|S_A - S_B|) \approx 73\ \mu$V/K, where $S_A (\approx +40\ \mu$V/K) and $S_B (\approx -33\ \mu$V/K) are obtained from the semi-classical Mott relation. The two other configurations (p–p and n–n) show a small thermovoltage with magnitudes close to zero because they destructively cancel each other. The coexistence of two opposite signs in p–p and n–n configurations is associated with the non-monotonicity of the thermovoltage in the gate voltage dependence of an individual graphene region (Fig. 2), resulting in six alternating signs in the thermovoltage map (marked as + and − for the sign).[31,32] This gate dependence demonstrates the good compatibility and functionality of the graphene thermocouple on the EVA/PET substrate endowed with parylene-N as a dielectric layer.

CONCLUSION

In summary, we demonstrated the realization of reliable, high-quality graphene-based field-effect devices on EVA/PET substrates using a convenient hot-press lamination transfer and parylene-N as a gate dielectric material. Using this technique, we developed a graphene thermocouple by placing two separate top gates in a single material graphene channel to modulate the carrier type and density in each region under the gate independently. Our findings suggest possible applications for producing scalable and reliable graphene-based thermoelectric devices on flexible and transparent substrates in a simple way. It can be employed particularly in sensitive opto-electronic measurements using photo-thermoelectric effects, where photon-excited changes in temperature induce a thermovoltage. Furthermore, by fabricating an array of graphene thermocouples on a large scale and placing them on a concave-shaped flexible substrate, the thermovoltage signal is highly amplified, and photon detection can be more effective.

ACKNOWLEDGMENTS

The financial support from the National Research Foundation of Korea (Grant Nos. NRF-2019R1C1C1003855, NRF-2019K1A3A1A47000489, and NRF-2022R1A4A3030766) is acknowledged. M.K. and A.Y. greatly appreciate the funding from the European Union's Horizon 2020 research and innovation program under the Marie Skłodowska-Curie Grant No. 955626 and the Nordic Programme for Interdisciplinary Research under Grant No. 105121, and the support from 2D Tech center (VINNOVA, Sweden) is greatly appreciated. This work was performed in part at Myfab Chalmers.

AUTHOR DECLARATIONS

Conflict of Interest

The authors have no conflicts to disclose.

Author Contributions

Youngwoo Nam: Writing – original draft (lead); Writing – review & editing (lead). **Daewon Gu**: Methodology (equal). **Munis Khan**: Methodology (equal). **August Yurgens**: Methodology (equal).

DATA AVAILABILITY

The data that support the findings of this study are available from the corresponding author upon reasonable request.

24 June 2024 10:38:33

© Author(s) 2024

REFERENCES

[1] A. K. Geim and I. V. Grigorieva, "van der Waals heterostructures," Nature **499**, 419–425 (2013).
[2] K. S. Novoselov, A. Mishchenko, A. Carvalho, and A. H. Castro Neto, "2D materials and van der Waals heterostructures," Science **353**, aac9439 (2016).
[3] P. Ajayan, P. Kim, and K. Banerjee, "Two-dimensional van der Waals materials," Phys. Today **69**(9), 38–44 (2016).
[4] P. Ares and K. S. Novoselov, "Recent advances in graphene and other 2D materials," Nano Mater. Sci. **4**, 3–9 (2022).
[5] Y. Nam, D.-K. Ki, D. Soler-Delgado, and A. F. Morpurgo, "A family of finite-temperature electronic phase transitions in graphene multilayers," Science **362**, 324–328 (2018).
[6] K. S. Novoselov, A. K. Geim, S. V. Morozov, D. Jiang, Y. Zhang, S. V. Dubonos, I. V. Grigorieva, and A. A. Firsov, "Electric field effect in atomically thin carbon films," Science **306**, 666–669 (2004).
[7] K. S. Novoselov, A. K. Geim, S. V. Morozov, D. Jiang, M. I. Katsnelson, I. V. Grigorieva, S. V. Dubonos, and A. A. Firsov, "Two-dimensional gas of massless Dirac fermions in graphene," Nature **438**, 197–200 (2005).
[8] K. S. Kim, Y. Zhao, H. Jang, S. Y. Lee, J. M. Kim, K. S. Kim, J.-H. Ahn, P. Kim, J.-Y. Choi, and B. H. Hong, "Large-scale pattern growth of graphene films for stretchable transparent electrodes," Nature **457**, 706–710 (2009).
[9] S. Bae, H. Kim, Y. Lee, X. Xu, J.-S. Park, Y. Zheng, J. Balakrishnan, T. Lei, H. Ri Kim, Y. I. Song, Y.-J. Kim, K. S. Kim, B. Özyilmaz, J.-H. Ahn, B. H. Hong, and S. Iijima, "Roll-to-roll production of 30-inch graphene films for transparent electrodes," Nat. Nanotechnol. **5**, 574–578 (2010).
[10] C. R. Dean, A. F. Young, I. Meric, C. Lee, L. Wang, S. Sorgenfrei, K. Watanabe, T. Taniguchi, P. Kim, K. L. Shepard, and J. Hone, "Boron nitride substrates for high-quality graphene electronics," Nat. Nanotechnol. **5**, 722–726 (2010).
[11] L. Wang, I. Meric, P. Y. Huang, Q. Gao, Y. Gao, H. Tran, T. Taniguchi, K. Watanabe, L. M. Campos, D. A. Muller, J. Guo, P. Kim, J. Hone, K. L. Shepard, and C. R. Dean, "One-dimensional electrical contact to a two-dimensional material," Science **342**, 614–617 (2013).
[12] V. P. Verma, S. Das, I. Lahiri, and W. Choi, "Large-area graphene on polymer film for flexible and transparent anode in field emission device," Appl. Phys. Lett. **96**, 203108 (2010).
[13] G. H. Han, H.-J. Shin, E. S. Kim, S. J. Chae, J.-Y. Choi, and Y. H. Lee, "Poly(ethylene co-vinyl acetate)-assisted one-step transfer of ultra-large graphene," Nano **06**, 59–65 (2011).
[14] B. N. Chandrashekar, B. Deng, A. S. Smitha, Y. Chen, C. Tan, H. Zhang, H. Peng, and Z. Liu, "Roll-to-roll green transfer of CVD graphene onto plastic for a transparent and flexible triboelectric nanogenerator," Adv. Mater. **27**, 5210–5216 (2015).
[15] M. Hempel, A. Y. Lu, F. Hui, T. Kpulun, M. Lanza, G. Harris, T. Palacios, and J. Kong, "Repeated roll-to-roll transfer of two-dimensional materials by electrochemical delamination," Nanoscale **10**, 5522–5531 (2018).
[16] I. A. Kostogrud, E. V. Boyko, and D. V. Smovzh, "The main sources of graphene damage at transfer from copper to PET/EVA polymer," Mater. Chem. Phys. **219**, 67–73 (2018).
[17] M. M. Tavakoli, G. Azzellino, M. Hempel, A.-Y. Lu, F. J. Martin-Martinez, J. Zhao, J. Yeo, T. Palacios, M. J. Buehler, and J. Kong, "Synergistic roll-to-roll transfer and doping of CVD-graphene using parylene for ambient-stable and ultra-lightweight photovoltaics," Adv. Funct. Mater. **30**, 2001924 (2020).
[18] M. Khan, K. Indykiewicz, P. L. Tam, and A. Yurgens, "High mobility graphene on EVA/PET," Nanomater. **12**, 331 (2022).
[19] D. Gu and Y. Nam, "Thermoelectric power measurements on graphite pencil lead and traces," J. Korean Phys. Soc. **83**, 978–983 (2023).
[20] G. Skoblin, J. Sun, and A. Yurgens, "Encapsulation of graphene in Parylene," Appl. Phys. Lett. **110**, 053504 (2017).
[21] X. Li, Y. Zhu, W. Cai, M. Borysiak, B. Han, D. Chen, R. D. Piner, L. Colombo, and R. S. Ruoff, "Transfer of large-area graphene films for high-performance transparent conductive electrodes," Nano Lett. **9**, 4359–4363 (2009).
[22] J. W. Suk, A. Kitt, C. W. Magnuson, Y. Hao, S. Ahmed, J. An, A. K. Swan, B. B. Goldberg, and R. S. Ruoff, "Transfer of CVD-grown monolayer graphene onto arbitrary substrates," ACS Nano **5**, 6916–6924 (2011).
[23] D. K. C. MacDonald, *Thermoelectricity: An Introduction to the Principles* (Dover Publications, 2006).
[24] Y. M. Zuev, W. Chang, and P. Kim, "Thermoelectric and magnetothermoelectric transport measurements of graphene," Phys. Rev. Lett. **102**, 096807 (2009).
[25] P. Wei, W. Bao, Y. Pu, C. N. Lau, and J. Shi, "Anomalous thermoelectric transport of Dirac particles in graphene," Phys. Rev. Lett. **102**, 166808 (2009).
[26] J. G. Checkelsky and N. P. Ong, "Thermopower and Nernst effect in graphene in a magnetic field," Phys. Rev. B **80**, 081413 (2009).
[27] G. Skoblin, J. Sun, and A. Yurgens, "Thermoelectric effects in graphene at high bias current and under microwave irradiation," Sci. Rep. **7**, 15542 (2017).
[28] A. Harzheim, F. Könemann, B. Gotsmann, H. van der Zant, and P. Gehring, "Single-material graphene thermocouples," Adv. Funct. Mater. **30**, 2000574 (2020).
[29] K. Kirihara, Y. Okigawa, M. Ishihara, M. Hasegawa, M. Mukaida, S. Horike, Y. Wang, and Q. Wei, "Transparent patternable large-area graphene p–n Junctions by photoinduced electron doping," ACS Appl. Mater. Interfaces **16**, 1198 (2023).
[30] S. Kim, S. Lim, M. H. Jeong, W. Kim, S. Baik, and J. W. Suk, "Flexible thermocouple using a thermoelectric graphene fiber with a seamless junction," J. Mater. Sci. Technol. **172**, 15–22 (2024).
[31] X. Xu, N. M. Gabor, J. S. Alden, A. M. van der Zande, and P. L. McEuen, "Photothermoelectric effect at a graphene interface junction," Nano Lett. **10**, 562–566 (2010).
[32] N. M. Gabor, J. C. W. Song, Q. Ma, N. L. Nair, T. Taychatanapat, K. Watanabe, T. Taniguchi, L. S. Levitov, and P. Jarillo-Herrero, "Hot carrier-assisted intrinsic photoresponse in graphene," Science **334**, 648–652 (2011).

24 June 2024 10:38:33

© Author(s) 2024